Scattering from frequency selective surfaces: A continuity condition for entire domain basis functions and an improved set of basis functions for crossed dipoles

Poulsen, Sören

1998

CODEN:LUTEDX/(TEAT-7073)/1-25/(1998)

Revision No. 1: October 1999

Scattering from frequency selective surfaces: A continuity condition for entire domain basis functions and an improved set of basis functions for crossed dipoles

Sören Poulsen

Electromagnetic Theory
Department of Electrical and Information Technology
Lund University
Sweden

Sören Poulsen (Soren.Poulsen@acab.se)

Applied Composites AB
P.O. Box 163
SE-341 23
Sweden

Editor: Gerhard Kristensson

Abstract

A plane wave impinges on an infinite, plane frequency selective surface (FSS) of patch type, and a surface current is induced on the conducting parts of the FSS. Using the established spectral Galerkin method, where the method of moment (MoM) procedure is carried out in the spectral domain, the induced current is determined, and the scattering problem is solved.

We derive a necessary continuity condition of entire domain basis functions, and show that basis functions which do not satisfy this condition are suppressed by the spectral Galerkin method. Specifically, we present an improved set of basis functions, designed for crossed dipoles. This set of basis functions consists of traditional even (symmetric) dipole basis functions, and a new set of V-dipole basis functions. It is found that the present basis functions are considerably more efficient than the existing basis functions for crossed dipoles. In fact, it is found that it suffices to take 4 of the present basis functions into account, still getting highly accurate result in a frequency band including the first two resonance frequencies.

1 Introduction

In 1984, Tsao and Mittra presented a method to calculate the scattered fields from frequency selective surfaces, which is sometimes referred to as the *spectral Galerkin method* [17]. In this method, the formulation is carried out in the spectral domain, where the convolution in the integral equation is reduced to an algebraic relation. The basis functions, used in the Galerkin's procedure, can be either entire domain or subdomain basis functions [18, 19]. The entire domain basis functions can be used successfully only on standard element geometries (such as crossed dipoles, Jerusalem crosses, circular rings, etc.), while the subdomain basis functions allow a general patch geometry. However, for standard element geometries, the entire domain basis functions are usually preferable, since the matrix to invert is usually much smaller than the subdomain one, and hence, the computation time is shorter. It is also well known that the double sum over the Floquet modes is usually more rapidly convergent in the entire domain case, also yielding shorter computation time [19].

The modes of resonance of the crossed dipole are well known [6, 10, 13, 14, 17]. Firstly, the fundamental resonance at f_1 corresponds to that observed for arrays of elements consisting of only (single) dipoles. Secondly, the resonance at f_2 arises through an asymmetric resonance in right-angle V-dipoles [14]. The surface current density that gives the first resonance at f_1 is accurately approximated by even (symmetric) dipole basis functions, *i.e.*, sine functions. However, the second one, f_2, is more troublesome. Hamdy and Parker [6] have found that, for their geometry, it is adequate to take 6 odd (asymmetric) dipole basis functions into account. However, in general, considerably more odd dipole basis functions are required to pick up the second resonance at f_2. In fact, for the geometry of Tsao and Mittra [17], we have found that 100 odd dipole basis functions are adequate.

Tsao and Mittra introduced a junction basis function to approximate the surface current density that gives the second resonance at f_2 [17]. In this paper, we derive

a necessary property of entire domain basis functions—a continuity condition—and show that basis functions which do not apply to this condition are suppressed by the spectral Galerkin method. This means that current coefficients corresponding to basis functions which do not obey to the continuity condition, which are obtained by matrix inversion, are small. Since the junction basis function of Tsao and Mittra is discontinuous, it does not apply to the continuity condition, and hence it is suppressed by the spectral Galerkin method. Basis functions which do not apply to the continuity condition have been used in the literature also on Jerusalem crosses [19]. Furthermore, existing entire domain bases for tripoles do not obey to the continuity condition [18].

In this paper, we introduce a new set of V-dipole basis functions. These basis functions are found to pick up the second resonance at f_2 excellently. Moreover, by numerical computations, it is found that it suffices to take only 4 of the present basis functions into account, still getting highly accurate result. The V-dipole basis functions are also applied to crossed dipoles with unequal lengths of the dipole arms, with applications to polarisation twisting reflectors [4].

In the next section we recapitulate the spectral Galerkin method. Then we derive the continuity condition and show that basis functions which do not apply to this continuity condition are suppressed by the spectral Galerkin method. After that, we present the improved set of basis functions and demonstrate their efficiency by several numerical computations of reflection and transmission coefficients. We consider both crossed dipoles with equal and unequal length of the dipole arms. Finally, the effect of reducing the length of one arm only is demonstrated.

2 Methods

Numerous methods have been used to analyse FSSs. Among other, we mention the equivalent circuit method, the mutual-impedance method and the integral equation method [19]. In this paper an integral equation method, called the spectral Galerkin method [17], is used to determine the scattered fields from the FSS. This is a spectral-domain approach where the convolution in the integral equation is reduced to an algebraic relation. It is important to notice that the forthcoming continuity condition is valid for the spectral Galerkin method, and that it is not applicable for the other methods, for instance, the equivalent circuit method.

In this section we review the spectral Galerkin method briefly, and introduce the notation of the forthcoming proof concerning the necessary properties of the entire domain basis functions.

2.1 The FSS and the incident field

The frequency selective surface (FSS) covers the plane $z = 0$. The periodic pattern is divided into identical cells, where the cell at the origin is called the *unit cell* E. The cartesian x-axis is directed along one of the periodic directions, and the y-axis is chosen so that x, y and z form a right hand system. Each cell, which

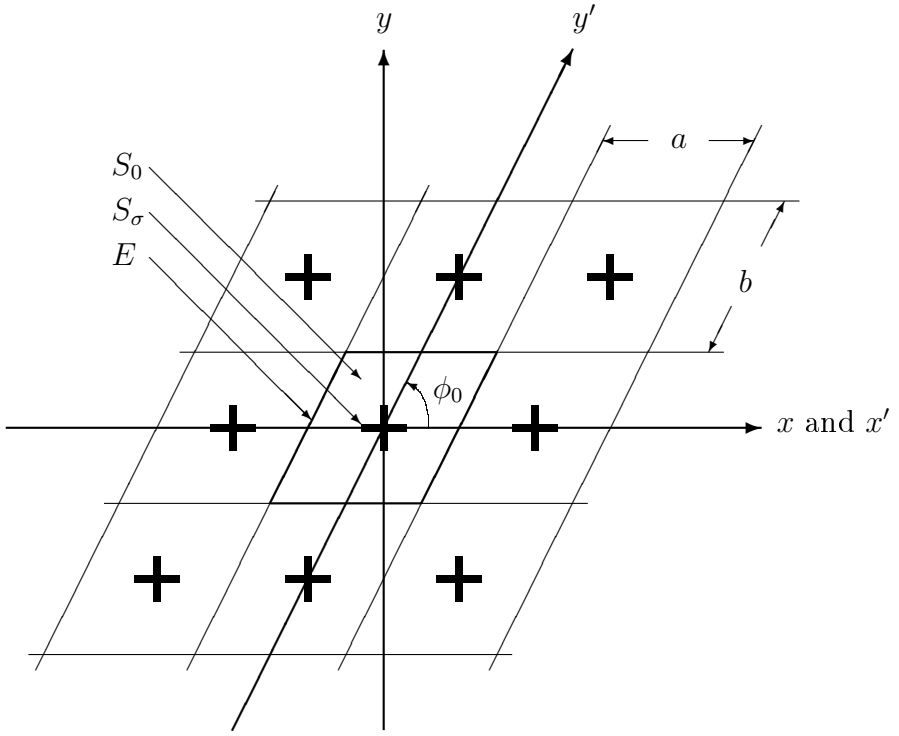

Figure 1: The unit cell E with the sides a and b.

is a parallelogram, has the sides a (along the x-axis) and b (in the other periodic direction). The angle between the two periodic directions is denoted ϕ_0, $0 < \phi_0 \leq \pi/2$, see Figure 1. Moreover, we introduce the area of the unit cell, denoted by $A_E := ab \sin \phi_0$. The unit cell is partly covered by a perfectly conducting, infinitely thin crossed dipole, and the set of points on this crossed dipole is denoted by S_σ (open set), while points in E, but outside the cross, are denoted S_0. Thus, we have $E = \overline{S_\sigma} \cup S_0$. We let $\hat{x}'$ and $\hat{y}'$ be unit vectors in the periodic directions, see Figure 1, so that

$$\begin{cases} x = x' + y' \cos \phi_0 \\ y = y' \sin \phi_0 \end{cases} \quad \begin{cases} x' = x - y \cot \phi_0 \\ y' = y / \sin \phi_0 \end{cases} \quad \begin{cases} \hat{x}' = \hat{x} \\ \hat{y}' = \hat{x} \cos \phi_0 + \hat{y} \sin \phi_0 \end{cases} \tag{2.1}$$

The incident field, $\boldsymbol{E}_i(\boldsymbol{r})$, is a plane wave with wave vector $\boldsymbol{k} = \hat{x} k \sin\theta \cos\phi + \hat{y} k \sin\theta \sin\phi + \hat{z} k \cos\theta$, where θ and ϕ are the spherical angles of the wave vector. The wave number k is defined as $k := \omega(\epsilon_0 \mu_0 \epsilon \mu)^{1/2}$, where $\omega := 2\pi f$ is the angular frequency, and f is the frequency. Here ϵ_0 and μ_0 are the free space permittivity and permeability, respectively, while ϵ and μ are the relative permittivity and permeability, respectively, of the surrounding space.

We assume that $0 \leq \theta < \pi/2$, *i.e.*, the incident plane wave impinges along the positive z axis. The incident plane wave can be written as

$$\boldsymbol{E}_i(\boldsymbol{r}) = \begin{cases} E_i \frac{\boldsymbol{k} \times \hat{z}}{|\boldsymbol{k} \times \hat{z}|} e^{i\boldsymbol{k}\cdot\boldsymbol{r}} = E_i \hat{e}_i^{\perp} e^{i\boldsymbol{k}\cdot\boldsymbol{r}} & \text{TE incidence} \\ E_i \frac{\boldsymbol{k} \times (\boldsymbol{k} \times \hat{z})}{|\boldsymbol{k} \times (\boldsymbol{k} \times \hat{z})|} e^{i\boldsymbol{k}\cdot\boldsymbol{r}} = E_i \hat{e}_i^{\parallel} e^{i\boldsymbol{k}\cdot\boldsymbol{r}} & \text{TM incidence} \end{cases}$$

where E_i is an complex constant. Note that the time convention $e^{-i\omega t}$ is adopted. The unit vectors of TE and TM incidence, respectively, are explicitely given by

$$\begin{cases} \hat{e}_i^{\perp} := \hat{x}\sin\phi - \hat{y}\cos\phi \\ \hat{e}_i^{\parallel} := \hat{x}\cos\theta\cos\phi + \hat{y}\cos\theta\sin\phi - \hat{z}\sin\theta \end{cases} \tag{2.2}$$

The orthogonal ($\perp$) and parallel ($\parallel$) symbols call attention to the fact that the electric field is orthogonal to the plane of incidence for TE polarization, while it is parallel to the plane of incidence for TM polarization. The transverse part of the incident electric field, denoted $\boldsymbol{E}_i^T(\boldsymbol{r})$, is easily obtained by subtracting the z component,

$$\boldsymbol{E}_i^T(\boldsymbol{r}) := (\overline{\overline{I}} - \hat{z}\hat{z}) \cdot \boldsymbol{E}_i(\boldsymbol{r}) = \boldsymbol{E}_i^T e^{i\boldsymbol{k}\cdot\boldsymbol{r}} \tag{2.3}$$

where $\overline{\overline{I}}$ is the three-dimensional unit dyadic, *i.e.*, $\overline{\overline{I}} := \hat{x}\hat{x} + \hat{y}\hat{y} + \hat{z}\hat{z}$, and where the polarisation vector is given by

$$\boldsymbol{E}_i^T := \begin{cases} E_i(\hat{x}\sin\phi - \hat{y}\cos\phi) & \text{TE incidence} \\ E_i\cos\theta(\hat{x}\cos\phi + \hat{y}\sin\phi) & \text{TM incidence} \end{cases}$$

This tangential electric field is used below when the system of linear equations for the induced current is derived.

2.2 Floquet expansion of the global current

When the incident plane wave impinges on the FSS, a current is induced in the perfectly conducting crossed dipoles. We assume that this current inherits the phase of the incident field. Then, the induced current $\boldsymbol{J}(\boldsymbol{\rho})$, which is defined for all $\boldsymbol{\rho} := \hat{x}x + \hat{y}y$, can be expanded according to Floquet's theorem [7] in *Floquet harmonics*:

$$\boldsymbol{J}(\boldsymbol{\rho}) = \sum_{m=-\infty}^{\infty}\sum_{n=-\infty}^{\infty} \boldsymbol{F}_{mn} e^{i\boldsymbol{\tau}_{mn}\cdot\boldsymbol{\rho}}, \quad \boldsymbol{\rho} \in \mathbb{R}^2 \tag{2.4}$$

where $\boldsymbol{\tau}_{mn} := \hat{x}\alpha_m + \hat{y}\beta_{mn}$ with

$$\alpha_m := \frac{2\pi m}{a} + k_x \qquad \beta_{mn} := \frac{2\pi n}{b\sin\phi_0} - \frac{2\pi m}{a}\cot\phi_0 + k_y$$

The real numbers k_x and k_y are the x and y components of the wave vector, respectively, and $\boldsymbol{F}_{mn}$ are the Floquet coefficients. The specific appearance of $\boldsymbol{\tau}_{mn}$ can be motivated in the following way. Let $\boldsymbol{\rho}$ be an arbitrary point in the unit cell E. By the relation (2.1), this point can be expressed in both the primed and the unprimed system of coordinates. We introduce the current $\boldsymbol{J}'(\boldsymbol{\rho}')$ as $\boldsymbol{J}'(\boldsymbol{\rho}') := \boldsymbol{J}(\boldsymbol{\rho})$, where $\boldsymbol{\rho}' = \hat{x}'x' + \hat{y}'y'$ and $\boldsymbol{\rho} = \hat{x}x + \hat{y}y$ denote the same vector. If we, as before, assume that the induced current inherits the phase of the incident field, the function $\boldsymbol{J}'(\boldsymbol{\rho}')e^{-i\boldsymbol{k}\cdot\boldsymbol{\rho}'}$ is periodic, with period a and b in the x' and y' direction, respectively. Hence, the function can be Fourier expanded as

$$\boldsymbol{J}'(\boldsymbol{\rho}')e^{-i\boldsymbol{k}\cdot\boldsymbol{\rho}'} = \sum_{m=-\infty}^{\infty}\sum_{n=-\infty}^{\infty} \boldsymbol{F}_{mn} e^{i2\pi mx'/a + i2\pi ny'/b}, \quad \boldsymbol{\rho}' \in \mathbb{R}^2$$

Since $\boldsymbol{\rho}' = \boldsymbol{\rho}$, we have $e^{i\boldsymbol{k}\cdot\boldsymbol{\rho}'} = e^{i\boldsymbol{k}\cdot\boldsymbol{\rho}}$, and the coordinate relation (2.1) then implies the Floquet expansion (2.4). To sum up, the Floquet expansion is nothing but an ordinary Fourier expansion in a non-orthogonal cartesian system of coordinates, under the assumption that the induced current inherits the phase of the incident field.

The spatial Fourier transform of the Floquet expanded current (2.4) is

$$\tilde{\boldsymbol{J}}(\boldsymbol{\tau}) = (2\pi)^2 \sum_{m=-\infty}^{\infty} \sum_{n=-\infty}^{\infty} \boldsymbol{F}_{mn} \delta^2(\boldsymbol{\tau} - \boldsymbol{\tau}_{mn}), \quad \boldsymbol{\tau} \in \mathbb{R}^2 \tag{2.5}$$

where the spectral variable is defined through $\boldsymbol{\tau} := \hat{x}\alpha + \hat{y}\beta$, and where $\delta^2(\boldsymbol{\tau}) := \delta(\alpha)\delta(\beta)$ is the two-dimensional delta function. The Fourier transform pair is

$$\begin{cases} \tilde{f}(\boldsymbol{\tau}) = \displaystyle\int_{\mathbb{R}^2} f(\boldsymbol{\rho}) e^{-i\boldsymbol{\tau}\cdot\boldsymbol{\rho}}\, dxdy \\ f(\boldsymbol{\rho}) = (2\pi)^{-2} \displaystyle\int_{\mathbb{R}^2} \tilde{f}(\boldsymbol{\tau}) e^{i\boldsymbol{\tau}\cdot\boldsymbol{\rho}}\, d\alpha d\beta \end{cases}$$

2.3 The unit cell current

We introduce the current $\boldsymbol{J}_E(\boldsymbol{\rho})$, which has support in the unit cell E, as $\boldsymbol{J}_E(\boldsymbol{\rho}) := \boldsymbol{J}(\boldsymbol{\rho})$ for all $\boldsymbol{\rho} \in E$. It is important to distinguish the two currents $\boldsymbol{J}(\boldsymbol{\rho})$ and $\boldsymbol{J}_E(\boldsymbol{\rho})$. On the unit cell E they are equal, but outside the unit cell $\boldsymbol{J}(\boldsymbol{\rho})$ is periodic, while $\boldsymbol{J}_E(\boldsymbol{\rho})$ vanishes. As a consequence, the Fourier spectrum of $\boldsymbol{J}(\boldsymbol{\rho})$ is discrete, see (2.5), while $\boldsymbol{J}_E(\boldsymbol{\rho})$ has a continuous spectrum.

We derive a relation between the Fourier coefficients of the global current $\boldsymbol{J}(\boldsymbol{\rho})$ and the Fourier transform of the unit cell current $\boldsymbol{J}_E(\boldsymbol{\rho})$. We start with the identity

$$\boldsymbol{J}_E(\boldsymbol{\rho}) = \boldsymbol{J}(\boldsymbol{\rho}), \quad \boldsymbol{\rho} \in E$$

If we multiply this equation by $e^{-i\boldsymbol{\tau}_{mn}\cdot\boldsymbol{\rho}}$, integrate over the unit cell, and substitute the Floquet harmonics expansion, (2.4), for $\boldsymbol{J}(\boldsymbol{\rho})$, we arrive at

$$\int_E \boldsymbol{J}_E(\boldsymbol{\rho}) e^{-i\boldsymbol{\tau}_{mn}\cdot\boldsymbol{\rho}}\, dxdy = \sum_{m'=-\infty}^{\infty} \sum_{n'=-\infty}^{\infty} \boldsymbol{F}_{m'n'} \int_E e^{i(\boldsymbol{\tau}_{m'n'} - \boldsymbol{\tau}_{mn})\cdot\boldsymbol{\rho}}\, dxdy, \quad (m,n) \in \mathbb{Z}^2$$

The integral on the left hand side can be extended from E to $\mathbb{R}^2$, due to the compact support of $\boldsymbol{J}_E(\boldsymbol{\rho})$ and it can be identified as the Fourier transform of the unit cell current $\tilde{\boldsymbol{J}}_E(\boldsymbol{\tau})$ evaluated at $\boldsymbol{\tau} = \boldsymbol{\tau}_{mn}$. On the other hand, the integral on the right hand side can be carried out after a substitution of the variables according to (2.1). We get

$$\int_E e^{i(\boldsymbol{\tau}_{m'n'} - \boldsymbol{\tau}_{mn})\cdot\boldsymbol{\rho}}\, dxdy = \int_0^a dx' \int_0^b \sin\phi_0\, dy' e^{2\pi i[(m'-m)x'/a + (n'-n)y'/b]} = A_E \delta_{m'm} \delta_{n'n}$$

where A_E is the area of the unit cell and where δ_{mn} is the Kronecker's delta, $\delta_{mn} = 1$ if $m = n$ and $\delta_{mn} = 0$ if $m \neq n$. Finally, we have

$$\widetilde{\boldsymbol{J}}_E(\boldsymbol{\tau}_{mn}) = A_E \boldsymbol{F}_{mn}, \quad (m,n) \in \mathbb{Z}^2 \tag{2.6}$$

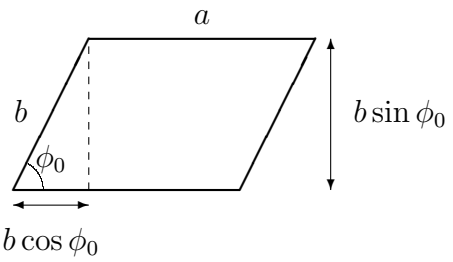

Figure 2: The distances $b\sin\phi_0$ and $b\cos\phi_0$.

This is the sought relation between the unit cell current and the global current. The relation is used later to eliminate the global current. The unit cell current can be approximated with arbitrary precision when it is expanded in a set of appropriate entire domain basis functions $\boldsymbol{j}_p(\boldsymbol{\rho})$, *i.e.*,

$$\boldsymbol{J}_E(\boldsymbol{\rho}) = \sum_{p\in\chi} C_p \boldsymbol{j}_p(\boldsymbol{\rho}) \tag{2.7}$$

where χ is a set of indicies and the scalars C_p are the unknown expansion coefficients. Here, the index p is an integer or a multi-index.

Finally, for completeness, an alternative derivation of (2.6) is now given [11]. The infinite number of periodic cells are numbered by indicies p and q, so that cell $(p+1,q)$ is the cell to the right (in the $\hat{x}'$ direction) of cell (p,q). Similarly, the cell $(p,q+1)$ is the cell above (in the $\hat{y}'$ direction) cell (p,q). We denote the current in cell (p,q) with $\boldsymbol{J}_{pq}(\boldsymbol{\rho})$. The current $\boldsymbol{J}_{pq}(\boldsymbol{\rho})$ vanishes outside cell (p,q). Furthermore, we let cell $(0,0)$ be the unit cell, that is $\boldsymbol{J}_{00}(\boldsymbol{\rho}) = \boldsymbol{J}_E(\boldsymbol{\rho})$. The current in cell (p,q), $\boldsymbol{J}_{pq}(\boldsymbol{\rho})$, can be related to the unit cell current by

$$\boldsymbol{J}_{pq}(\boldsymbol{\rho}) = \boldsymbol{J}_E(\boldsymbol{\rho}-\boldsymbol{\rho}_{pq})e^{i\boldsymbol{k}\cdot\boldsymbol{\rho}_{pq}}, \quad \boldsymbol{\rho}\in\mathbb{R}^2$$

where $\boldsymbol{\rho}_{pq} := \hat{x}(pa+qb\cos\phi_0)+\hat{y}qb\sin\phi_0$. Note that this relation is based upon the assumption that the induced current inherits the phase of the incident field. The origin of the different factors in the translation vector $\boldsymbol{\rho}_{pq}$ is illustrated in Figure 2.

The global current $\boldsymbol{J}(\boldsymbol{\rho})$ now reads

$$\boldsymbol{J}(\boldsymbol{\rho}) = \sum_{p=-\infty}^{\infty}\sum_{q=-\infty}^{\infty} \boldsymbol{J}_{pq}(\boldsymbol{\rho}) = \sum_{p=-\infty}^{\infty}\sum_{q=-\infty}^{\infty} \boldsymbol{J}_E(\boldsymbol{\rho}-\boldsymbol{\rho}_{pq})e^{i\boldsymbol{k}\cdot\boldsymbol{\rho}_{pq}}, \quad \boldsymbol{\rho}\in\mathbb{R}^2$$

By taking the spatial Fourier transform of this equation, we arrive at

$$\widetilde{\boldsymbol{J}}(\boldsymbol{\tau}) = \widetilde{\boldsymbol{J}}_E(\boldsymbol{\tau}) \sum_{p=-\infty}^{\infty}\sum_{q=-\infty}^{\infty} e^{i(\boldsymbol{k}-\boldsymbol{\tau})\cdot\boldsymbol{\rho}_{pq}}, \quad \boldsymbol{\tau}\in\mathbb{R}^2$$

where, as before, $\boldsymbol{\tau} = \hat{x}\alpha+\hat{y}\beta$ is the spectral variable. We first use the formula $\sum_{p=-\infty}^{\infty} e^{-ipx} = 2\pi\sum_{m=-\infty}^{\infty}\delta(x-2\pi m)$ to replace the exponential function, and

then, we use the relation $\delta(ax) = \delta(x)/|a|$ to extract a and $b\sin\phi_0$, yielding $1/A_E$. The final result is

$$\widetilde{\boldsymbol{J}}(\boldsymbol{\tau}) = \widetilde{\boldsymbol{J}}_E(\boldsymbol{\tau})\frac{(2\pi)^2}{A_E}\sum_{m=-\infty}^{\infty}\sum_{n=-\infty}^{\infty}\delta^2(\boldsymbol{\tau}-\boldsymbol{\tau}_{mn}), \quad \boldsymbol{\tau}\in\mathbb{R}^2 \tag{2.8}$$

were, as before, $\boldsymbol{\tau}_{mn} = \hat{x}\alpha_m + \hat{y}\beta_{mn}$. Now, the sought relation (2.6) immediately follows from (2.5).

2.4 The scattering operator

In this subsection, we derive the scattering operator, *i.e.*, the operator which for a known current gives the scattered field. It is well known that the scattered field is given by the convolution integral [19]

$$\boldsymbol{E}(\boldsymbol{r}) = -\frac{1}{i\omega\epsilon_0\epsilon}[k^2\overline{\overline{I}}_2 + \nabla\nabla]\cdot\int_{\mathbb{R}^2} g(\boldsymbol{r}-\boldsymbol{\rho}')\boldsymbol{J}(\boldsymbol{\rho}')\,dx'dy', \quad z\neq 0 \tag{2.9}$$

where $\overline{\overline{I}}_2 := \hat{x}\hat{x} + \hat{y}\hat{y}$, and where the free space Green's function $g(\boldsymbol{r}) := e^{ik|\boldsymbol{r}|}/4\pi|\boldsymbol{r}|$ is a solution to the Helmholtz' equation,

$$(\nabla^2 + k^2)g(\boldsymbol{r}) = -\delta^3(\boldsymbol{r}) \tag{2.10}$$

The convolution integral, (2.9), defines the scattering operator for the global current. In the spectral Galerkin method, which we use here, it is the unit cell current, and not the global current, which is expanded in basis functions. Thus, we need the scattering operator for the unit cell current. By taking the spatial Fourier transform of the convolution integral (2.9) in the transverse coordinates $\boldsymbol{\rho}$, we arrive at

$$\tilde{\boldsymbol{E}}(\boldsymbol{\tau}, z) = -\frac{1}{i\omega\epsilon_0\epsilon}[k^2\overline{\overline{I}}_2 - \boldsymbol{\tau}\boldsymbol{\tau} + i\frac{\partial}{\partial z}\hat{z}\boldsymbol{\tau}]\cdot\tilde{g}(\boldsymbol{\tau}, z)\tilde{\boldsymbol{J}}(\boldsymbol{\tau}), \quad z\neq 0 \tag{2.11}$$

where $\tilde{g}(\boldsymbol{\tau}, z)$ is the Fourier transform of the free space Green's function. Note that the Fourier transform converts the convolution integral to an ordinary multiplication. To derive $\tilde{g}(\boldsymbol{\tau}, z)$, we start with the Fourier transform of the Helmholtz' equation (2.10), which reads,

$$\left(\gamma^2 + \frac{\partial^2}{\partial z^2}\right)\tilde{g}(\boldsymbol{\tau}, z) = -\delta(z)$$

where γ is defined through $k^2 = |\boldsymbol{\tau}|^2 + \gamma^2$. Here, the principal square root branch is chosen such that the imaginary part of γ is non-negative. The above ordinary differential equation is solved for $z < 0$ and $z > 0$, respectively, and the following boundary conditions are applied,

$$\begin{cases} \lim\limits_{\varepsilon\to 0+}[g(\boldsymbol{\rho}+\hat{z}\varepsilon) - g(\boldsymbol{\rho}-\hat{z}\varepsilon)] = 0 \\ \lim\limits_{\varepsilon\to 0+}\dfrac{\partial}{\partial z}[g(\boldsymbol{\rho}+\hat{z}\varepsilon) - g(\boldsymbol{\rho}-\hat{z}\varepsilon)] = -1 \end{cases}$$

In the latter boundary condition, it is understood that the derivative with respect to z is done before the limiting process. Moreover, the solution should be an outgoing wave in each half space, respectively. The result is

$$\tilde{g}(\boldsymbol{\tau}, z) = \frac{i}{2\gamma} e^{i\gamma|z|}$$

Our next move is to replace the global current in (2.11) by the unit cell current by using (2.5) and (2.6), and then apply the inverse Fourier transform, to obtain

$$\boldsymbol{E}(\boldsymbol{r}) = -\frac{1}{i\omega\epsilon_0\epsilon A_E} \sum_{m=-\infty}^{\infty} \sum_{n=-\infty}^{\infty} \tilde{g}(\boldsymbol{\tau}_{mn}, z) \overline{\overline{G}}_{mn}(z) \cdot \tilde{\boldsymbol{J}}_E(\boldsymbol{\tau}_{mn}) e^{i\boldsymbol{\tau}_{mn}\cdot\boldsymbol{\rho}}, \quad z \neq 0 \quad (2.12)$$

where $\overline{\overline{G}}_{mn}(z) := k^2\overline{\overline{I}}_2 - \boldsymbol{\tau}_{mn}\boldsymbol{\tau}_{mn} - \gamma_{mn}\,\mathrm{sgn}(z)\hat{z}\boldsymbol{\tau}_{mn}$. Here $\mathrm{sgn}(z)$ is the sign function, that is $\mathrm{sgn}(z)$ gives -1 or 1 depending on whether z is negative or positive. The scalar γ_{mn} is defined by $\gamma_{mn} := (k^2 - |\boldsymbol{\tau}_{mn}|^2)^{1/2}$. As before, the principal square root branch is chosen such that the imaginary part of γ_{mn} is non-negative.

It is evident from (2.12) that the scattered field is a discrete sum of plane waves. Some of these are propagating waves, while others are evanescent waves (inhomogeneous waves). For instance, the wave corresponding to $m = n = 0$, for positive z, is a plane wave propagating in the transmitted direction, *i.e.*, in the $\boldsymbol{k}_t := \boldsymbol{k}$ direction. On the other hand, for negative z, the wave corresponding to $m = n = 0$, is a plane wave propagating in the reflected direction, *i.e.*, in the $\boldsymbol{k}_r := (\overline{\overline{I}} - 2\hat{z}\hat{z}) \cdot \boldsymbol{k}$ direction, where $\overline{\overline{I}}$ is the three-dimensional unit dyadic. For sufficiently large m and n, the corresponding plane wave has an exponential decay in the $\pm z$ direction, due to behaviour of $\tilde{g}(\boldsymbol{\tau}_{mn}, z)$, and this wave is evanescent. To sum up, the scattered field consists of a finite number of propagating plane waves, and an infinite number of evanescent plane waves.

2.5 The linear system of equations for the unit cell current

Following the Galerkin procedure, it is quite straightforward to derive a system of linear equations for the unit cell current from (2.12). Since the total tangential electric field vanishes on a conductor, we have[1]

$$\boldsymbol{E}_i^T(\boldsymbol{\rho}) = \frac{\eta_0\eta}{2kA_E} \sum_{m=-\infty}^{\infty} \sum_{n=-\infty}^{\infty} \overline{\overline{g}}_{mn} \cdot \tilde{\boldsymbol{J}}_E(\boldsymbol{\tau}_{mn}) e^{i\boldsymbol{\tau}_{mn}\cdot\boldsymbol{\rho}}, \quad \boldsymbol{\rho} \in S_\sigma$$

where $\eta_0 := (\mu_0/\epsilon_0)^{1/2}$ is the impedance of free space, $\eta := (\mu/\epsilon)^{1/2}$ is the relative impedance, and where

$$\overline{\overline{g}}_{mn} = \frac{1}{\gamma_{mn}}(k^2\overline{\overline{I}}_2 - \boldsymbol{\tau}_{mn}\boldsymbol{\tau}_{mn})$$

The transverse part of the incident field, $\boldsymbol{E}_i^T(\boldsymbol{\rho})$, is defined through (2.3). We multiply the above equation by $\boldsymbol{j}_q^*(\boldsymbol{\rho})\cdot$, where $*$ denotes the complex conjugate, and

[1] Taking the limit $|z| \to 0$ of the tangential part of (2.12) we obtain a well-defined limit [3].

integrate over the conducting part of the unit cell S_σ. Then, the left and right hand side can be identified as a Fourier transform, *i.e.*,

$$\tilde{\boldsymbol{j}}_q^*(\boldsymbol{k}^T)\cdot\boldsymbol{E}_i^T = \frac{\eta_0\eta}{2kA_E}\sum_{m=-\infty}^{\infty}\sum_{n=-\infty}^{\infty}\tilde{\boldsymbol{j}}_q^*(\boldsymbol{\tau}_{mn})\cdot\overline{\overline{g}}_{mn}\cdot\tilde{\boldsymbol{J}}_E(\boldsymbol{\tau}_{mn}),\quad q\in\chi$$

where the transversal wave vector is defined by $\boldsymbol{k}^T := \overline{\overline{I}}_2\cdot\boldsymbol{k}$. Finally, we replace the unit cell current with its basis function expansion (2.7). We have

$$\tilde{\boldsymbol{j}}_q^*(\boldsymbol{k}^T)\cdot\boldsymbol{E}_i^T = \frac{\eta_0\eta}{2kA_E}\sum_{p\in\chi}C_p\sum_{m=-\infty}^{\infty}\sum_{n=-\infty}^{\infty}\tilde{\boldsymbol{j}}_q^*(\boldsymbol{\tau}_{mn})\cdot\overline{\overline{g}}_{mn}\cdot\tilde{\boldsymbol{j}}_p(\boldsymbol{\tau}_{mn}) \tag{2.13a}$$

where $q\in\chi$. If χ is an infinite set of indicies, the above equation is an infinite system of linear equations for the unknown current coefficients C_p. We assume that if this infinite system is truncated, the solution to the truncated system approximates the exact solution. When the linear system (2.13a) is truncated, it can be written

$$\mathbf{A}\boldsymbol{C} = \boldsymbol{b} \tag{2.13b}$$

where $\mathbf{A}$ is a square matrix and $\boldsymbol{C}$ is a vector containing the unknown coefficients C_p. The following properties of the linear system of equations are obvious:

- The size of the matrix equals the number of basis functions used, *i.e.*, the number of elements in χ.
- The matrix has to be computed for each frequency.
- The matrix is not dependent on the polarization of the incident field, but it depends on the angles of incidence.
- The truncation of the infinite sums depends on the asymptotic behaviour of $\tilde{\boldsymbol{j}}_p(\boldsymbol{\tau}_{mn})$ for large $|m|$ and $|n|$.

According to the "phenomenon of relative convergence" [8, 15], for some geometries and for a fixed number of basis functions, there is an optimal truncation of the double sum of Floquet modes. In other words, for some geometries, the number of terms in the double sum can be related to the number of basis functions used. However, in general, we gradually increase the number of terms until the matrix elements converge.

2.6 The reflection and transmission coefficients

Once the linear system is solved, the unit cell current is known, and the scattered field is given by (2.12). We have seen that the scattered field consists of at least two propagating plane waves, one of which propagates in the reflected direction $\boldsymbol{k}_r$,

and one of which propagates in the transmitted direction $\boldsymbol{k}_t$. We denote these plane waves by $\boldsymbol{E}_r(\boldsymbol{r})$ and $\boldsymbol{E}_t(\boldsymbol{r})$, respectively, *i.e.*,

$$\begin{aligned}\boldsymbol{E}_r(\boldsymbol{r}) &:= -\frac{1}{i\omega\epsilon_0\epsilon A_E}\tilde{g}(\boldsymbol{\tau}_{00}, z)\overline{\overline{G}}_{00}(z)\cdot\tilde{\boldsymbol{J}}_E(\boldsymbol{\tau}_{00})e^{i\boldsymbol{\tau}_{00}\cdot\boldsymbol{\rho}}, \quad z<0\\ \boldsymbol{E}_t(\boldsymbol{r}) &:= -\frac{1}{i\omega\epsilon_0\epsilon A_E}\tilde{g}(\boldsymbol{\tau}_{00}, z)\overline{\overline{G}}_{00}(z)\cdot\tilde{\boldsymbol{J}}_E(\boldsymbol{\tau}_{00})e^{i\boldsymbol{\tau}_{00}\cdot\boldsymbol{\rho}}, \quad z>0\end{aligned}$$

which can be simplified to

$$\begin{aligned}\boldsymbol{E}_r(\boldsymbol{r}) &= -\frac{\eta_0\eta}{2kk_zA_E}\overline{\overline{G}}^{-}_{00}\cdot\tilde{\boldsymbol{J}}_E(\boldsymbol{k}^T)e^{i\boldsymbol{k}_r\cdot\boldsymbol{r}} = \boldsymbol{E}_r e^{i\boldsymbol{k}_r\cdot\boldsymbol{r}}\\ \boldsymbol{E}_t(\boldsymbol{r}) &= -\frac{\eta_0\eta}{2kk_zA_E}\overline{\overline{G}}^{+}_{00}\cdot\tilde{\boldsymbol{J}}_E(\boldsymbol{k}^T)e^{i\boldsymbol{k}_t\cdot\boldsymbol{r}} = \boldsymbol{E}_t e^{i\boldsymbol{k}_t\cdot\boldsymbol{r}}\end{aligned} \tag{2.14}$$

where $\overline{\overline{G}}^{\pm}_{00} := k^2\overline{\overline{I}}_2 - \boldsymbol{k}^T\boldsymbol{k}^T \mp k_z\hat{z}\boldsymbol{k}^T$ and where k_z is the z component of the wave vector, $k_z := \hat{z}\cdot\boldsymbol{k} > 0$. Here, $\boldsymbol{E}_r$ and $\boldsymbol{E}_t$ are the amplitude and polarization of the reflected and transmitted plane waves, respectively. We determine these amplitudes for the TE and TM polarization of the incident field, respectively, and obtain the amplitudes $\boldsymbol{E}_r^{\perp}$, $\boldsymbol{E}_r^{\parallel}$, $\boldsymbol{E}_t^{\perp}$, and $\boldsymbol{E}_t^{\parallel}$. Note that since the matrix in the system of linear equations, (2.13b), is independent of the polarization of the incident field, these four amplitudes are determined by a single matrix inversion.

We define the unit vectors for TE and TM polarization of the transmitted field, respectively, see (2.2),

$$\hat{e}_t^{\perp} := \hat{e}_i^{\perp} \quad \text{and} \quad \hat{e}_t^{\parallel} := \hat{e}_i^{\parallel}$$

Similarly, the unit vectors for the reflected field are

$$\hat{e}_r^{\perp} := -\hat{e}_i^{\perp} \quad \text{and} \quad \hat{e}_r^{\parallel} := (2\hat{z}\hat{z} - \overline{\overline{I}})\cdot\hat{e}_i^{\parallel}$$

The dyadic $2\hat{z}\hat{z} - \overline{\overline{I}}$, leaves the z component of $\hat{e}_i^{\parallel}$ unaltered, while it changes the signs of the x and y components, see also Figure 3.

In general, the FSS generates a cross-polarized component of the reflected and transmitted fields. For instance, if the incident field is TE polarized, the transmitted field is not necessarily strictly TE polarized. Therefore, we introduce four reflection coefficients, $R^{\perp\perp}$, $R^{\perp\parallel}$, $R^{\parallel\perp}$ and $R^{\parallel\parallel}$, and four transmission coefficients, $T^{\perp\perp}$, $T^{\perp\parallel}$, $T^{\parallel\perp}$ and $T^{\parallel\parallel}$. Here the first symbol in each pair refers to the polarization of the incident field, while the second refers to the polarization of the reflected and transmitted fields, respectively. The coefficients are complex. Without loss of generality, we assume that the incident field is of unit strength, that is $E_i = 1$. The reflection coefficients are given by

$$\begin{aligned} R^{\perp\perp} &:= \boldsymbol{E}_r^{\perp}\cdot\hat{e}_r^{\perp} & R^{\parallel\perp} &:= \boldsymbol{E}_r^{\parallel}\cdot\hat{e}_r^{\perp}\\ R^{\perp\parallel} &:= \boldsymbol{E}_r^{\perp}\cdot\hat{e}_r^{\parallel} & R^{\parallel\parallel} &:= \boldsymbol{E}_r^{\parallel}\cdot\hat{e}_r^{\parallel}\end{aligned}$$

Since the transmitted field is the total field for $z > 0$, the incident field has to be added, and the transmission coefficients are given by

$$\begin{aligned} T^{\perp\perp} &:= \boldsymbol{E}_t^{\perp}\cdot\hat{e}_t^{\perp} + 1 & T^{\parallel\perp} &:= \boldsymbol{E}_t^{\parallel}\cdot\hat{e}_t^{\perp}\\ T^{\perp\parallel} &:= \boldsymbol{E}_t^{\perp}\cdot\hat{e}_t^{\parallel} & T^{\parallel\parallel} &:= \boldsymbol{E}_t^{\parallel}\cdot\hat{e}_t^{\parallel} + 1\end{aligned}$$

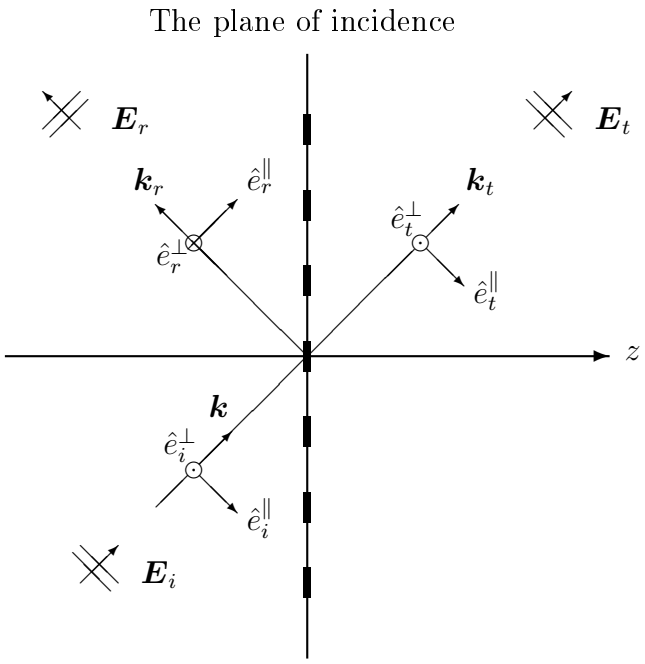

Figure 3: The reflected and transmitted field.

The scattered field $\boldsymbol{E}(\boldsymbol{r})$ depends of course on the specific form of the unit cell current, but the coefficients above depends only on the slow oscillations of the unit cell current. This is concluded from (2.14), where it is evident that only $\tilde{\boldsymbol{J}}_E(\boldsymbol{k}^T)$ contributes.

2.7 The continuity condition

We start with the p:th diagonal element of the linear system (2.13b), which is

$$a_{pp} := \sum_{m=-\infty}^{\infty} \sum_{n=-\infty}^{\infty} d_{mn} \tag{2.15}$$

where $d_{mn} := \tilde{\boldsymbol{j}}_p^*(\boldsymbol{\tau}_{mn}) \cdot \overline{\overline{g}}_{mn} \cdot \tilde{\boldsymbol{j}}_p(\boldsymbol{\tau}_{mn})$. By straightforward calculations we find that

$$\begin{aligned} d_{mn} = \frac{1}{\sqrt{k^2 - \alpha_m^2 - \beta_{mn}^2}} \big(& |\tilde{j}_x(\alpha_m, \beta_{mn})|^2 (k^2 - \alpha_m^2) \\ & -2\alpha_m \beta_{mn} \operatorname{Re}\{\tilde{j}_x^*(\alpha_m, \beta_{mn}) \tilde{j}_y(\alpha_m, \beta_{mn})\} + |\tilde{j}_y(\alpha_m, \beta_{mn})|^2 (k^2 - \beta_{mn}^2) \big) \end{aligned}$$

where $\tilde{\boldsymbol{j}}_p(\boldsymbol{\tau}) = \hat{x}\tilde{j}_x(\alpha, \beta) + \hat{y}\tilde{j}_y(\alpha, \beta)$. First we examine the asymptotic behaviour of d_{mn} for large β_{mn}. For fixed $m = m'$, $\beta_{m'n} = O(\nu n)$ where $\nu := 2\pi/b \sin\phi_0$, and we have

$$\begin{aligned} d_{m'n} \propto \frac{1}{i\nu n} & |\tilde{j}_x(\alpha_{m'}, \nu n)|^2 (k^2 - \alpha_{m'}^2) + 2i\alpha_{m'} \operatorname{Re}\{\tilde{j}_x^*(\alpha_{m'}, \nu n) \tilde{j}_y(\alpha_{m'}, \nu n)\} \\ & + i\nu n \, |\tilde{j}_y(\alpha_{m'}, \nu n)|^2 \end{aligned}$$

for large $|n|$. This means that if $\tilde{j}_x(\alpha_{m'}, \nu n) = O(n^{1-l})$ or $\tilde{j}_y(\alpha_{m'}, \nu n) = O(n^{-l})$, for large $|n|$, any $l \leq 1$, then the sum over n in (2.15) diverges for each $m = m'$. Next we examine the asymptotic behaviour of d_{mn} for large α_m. For large $|m|$ and $|n|$ in the strip $|n - mb\cos\phi_0/a| \leq \varepsilon$, where $\varepsilon > 0$ is constant, $\alpha_m = O(\eta m)$ where $\eta := 2\pi/a$, and we have

$$d_{mn} \propto i\eta m\,|\tilde{j}_x(\eta m, \beta_{mn})|^2 + 2i\beta_{mn}\,\mathrm{Re}\{\tilde{j}_x^*(\eta m, \beta_{mn})\tilde{j}_y(\eta m, \beta_{mn})\} + \frac{1}{i\eta m}|\tilde{j}_y(\eta m, \beta_{mn})|^2(k^2 - \beta_{mn}^2)$$

This means that if $\tilde{j}_x(\eta m, \beta_{mn}) = O(m^{-l})$ or $\tilde{j}_y(\eta m, \beta_{mn}) = O(m^{1-l})$, for large $|m|$ and $|n|$ in the strip $|n - mb\cos\phi_0/a| \leq \varepsilon$, any $l \leq 1$, then the sum in (2.15) diverges. Note that β_{mn} is bounded in the strip.

To sum up, if $\tilde{\boldsymbol{j}}_p(\boldsymbol{\tau}) = \hat{x}\tilde{j}_x(\alpha, \beta) + \hat{y}\tilde{j}_y(\alpha, \beta)$ is an arbitrary entire domain basis function, then the corresponding double infinite sum of Floquet modes, (2.15), which occurs as the p:th diagonal element of the linear system (2.13b), diverges if either

$$\tilde{j}_x(\alpha, \beta') = O(\alpha^{-l}) \quad \text{for large } |\alpha|,\ \beta' \text{ fixed, any } l \leq 1 \tag{2.16a}$$

$$\tilde{j}_y(\alpha', \beta) = O(\beta^{-l}) \quad \text{for large } |\beta|,\ \alpha' \text{ fixed, any } l \leq 1 \tag{2.16b}$$

$$\tilde{j}_x(\alpha', \beta) = O(\beta^{-l}) \quad \text{for large } |\beta|,\ \alpha' \text{ fixed, any } l \leq 0 \tag{2.16c}$$

or

$$\tilde{j}_y(\alpha, \beta') = O(\alpha^{-l}) \quad \text{for large } |\alpha|,\ \beta' \text{ fixed, any } l \leq 0 \tag{2.16d}$$

Consider a discontinuous function $j(x) : \mathbb{R} \to \mathbb{R}$, which has support in the interval $(x_1, x_2) \subset \mathbb{R}$. Without loss of generality, we suppose that $j(x)$ is discontinuous in only one point, $x_1 < x_0 < x_2$ say, and that it is continuous elsewhere. The function $j(x)$ can be decomposed in one continuous function $j_c(x)$ and a Heaviside function,

$$j(x) = j_c(x) + \Delta H(x - x_0)$$

where $j_c(x)$ is continuous on (x_1, x_2) and Δ is the jump discontinuity at $x = x_0$. It is well known [16] that the Fourier transform of the Heaviside function decays as $\tilde{H}(\alpha) \propto 1/\alpha$ for large $|\alpha|$. Thus, $\tilde{j}(\alpha) = O(\alpha^{-1})$ for large $|\alpha|$. From (2.16a) and (2.16b) it is concluded that if the basis function $\boldsymbol{j}_p(\boldsymbol{\rho}) = \hat{x}j_x^x(x)j_x^y(y) + \hat{y}j_y^x(x)j_y^y(y)$ not obeys to the following *continuity condition*,

$$\begin{cases} j_x^x(x) : \mathbb{R} \to \mathbb{R} \text{ is continuous} \\ j_y^y(y) : \mathbb{R} \to \mathbb{R} \text{ is continuous} \end{cases} \tag{2.17}$$

then the corresponding double infinite sum, (2.15), is divergent. Note that continuity of $j_x^y(y)$ and $j_y^x(x)$ is not demanded, but that a restriction in the singularity of these functions can be derived from (2.16c) and (2.16d). Moreover, note that the continuity condition, (2.17), is valid only for separable basis functions, *i.e.*, basis functions which can be written $\boldsymbol{j}_p(\boldsymbol{\rho}) = \hat{x}j_x^x(x)j_x^y(y) + \hat{y}j_y^x(x)j_y^y(y)$. For a non-separable basis

function, $\boldsymbol{j}_p(\boldsymbol{\rho}) = \hat{x} j_x(x,y) + \hat{y} j_y(x,y)$, the situation is more complicated, and we refer to the conditions (2.16a)–(2.16d).

Finally, we sketch how basis functions which do not fulfill the continuity condition are handled by the spectral Galerkin method. Suppose that the basis function $\boldsymbol{j}_p(\boldsymbol{\rho})$ does not obey to the continuity condition, and that all matrix elements a_{pq} in (2.13b) are bounded, except for a_{pp}. Since the continuity condition is not fulfilled, the double infinite sum (2.15) is divergent. The unknown current coefficient C_p in (2.13b) is given by Cramer's rule [12] as

$$C_p = \frac{\det \mathbf{A}_p}{\det \mathbf{A}}$$

where $\mathbf{A}_p$ is the matrix $\mathbf{A}$ with its p:th column replaced by the right-hand side $\boldsymbol{b}$. Since $\det \mathbf{A}_p$ is bounded, while $\det \mathbf{A}$ is infinite, the current coefficient C_p is zero. Thus, basis functions which do not fulfill the continuity condition are suppressed by the spectral Galerkin method. However, if we truncate the divergent, double infinite sum, the current coefficient C_p is not identically zero, but its value is strongly dependent of the choice of truncation.

3 Results

In the above analysis, the free space Green's function was used, and hence the FSS has no kind of dielectric support. However, a multi-layer dielectric support can be handled by an appropriate Green's function. For instance, this Green's function can be calculated by the G1DMULT routine [9].

The junction basis function given by Tsao and Mittra [17] does not obey the continuity condition, and hence it is not pertinent. Numerically, this shows up when we try to find an appropriate truncation of the Floquet sum corresponding to the junction basis function, since this sum is divergent. We have also, unsuccessfully, tried to use a more general projection method than the Galerkin procedure and used another testing function corresponding to the junction basis function. Moreover, it is found that the convergence of the MoM solution is very slow, when ordinary even and odd dipole basis functions are used. In fact, from Figure 7 it is evident that we need about 100 odd dipole basis function to accurately approximate the surface current that gives the second resonance at f_2.

In view of this, we develop a new set of basis functions for crossed dipoles. It is found that the surface current density that gives the first resonance mode at f_1 is well approximated by the ordinary even dipole basis functions (see (3.1) below), and that it is the second resonace at f_2, occuring in right-angle V-dipoles, which is troublesome. However, following the idea of Tsao and Mittra, we design a new set of V-dipole basis functions—which obeys the continuity condition—to approximate the surface current density that gives the second resonance at f_2.

3.1 An improved set of basis functions

We denote the length and the width of the dipole arms by L and W, respectively, see Figure 4.

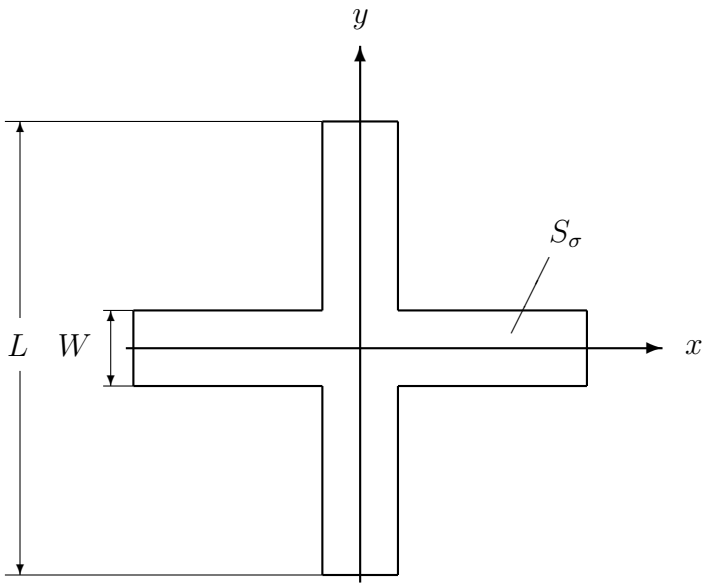

Figure 4: A crossed dipole. Note the length (L) and width (W) of the arms.

Firstly, the following traditional even dipole basis functions are defined:

$$\begin{aligned} \boldsymbol{j}_p^1(\boldsymbol{\rho}) &:= \hat{x}\sin(\pi(2p-1)(x+L/2)/L), \quad \boldsymbol{\rho} \text{ on the } x \text{ arm} \\ \boldsymbol{j}_p^2(\boldsymbol{\rho}) &:= \hat{y}\sin(\pi(2p-1)(y+L/2)/L), \quad \boldsymbol{\rho} \text{ on the } y \text{ arm} \end{aligned} \tag{3.1}$$

Here, and in the following definitions, it is understood that the basis functions have support on the conducting part of the crossed dipole. Moreover, we define the V-dipole basis functions (here $(x,y) \in S_\sigma$)

$$\boldsymbol{j}_p^3(\boldsymbol{\rho}) := \begin{cases} \hat{x}A_p(x,y) & x > W/2 \\ -\hat{y}A_p(y,x) & y > W/2 \\ \hat{x}s(x)c(y) - \hat{y}c(x)s(y) & |x| \le W/2 \text{ and } |y| \le W/2 \end{cases}$$

$$\boldsymbol{j}_p^4(\boldsymbol{\rho}) := \begin{cases} -\hat{x}A_p(-x,-y) & x < -W/2 \\ \hat{y}A_p(-y,-x) & y < -W/2 \\ -\hat{x}c(x)s(y) + \hat{y}s(x)c(y) & |x| \le W/2 \text{ and } |y| \le W/2 \end{cases}$$

$$\boldsymbol{j}_p^5(\boldsymbol{\rho}) := \begin{cases} -\hat{x}A_p(-x,y) & x < -W/2 \\ -\hat{y}A_p(y,-x) & y > W/2 \\ -\hat{x}s(-x)c(y) - \hat{y}c(-x)s(y) & |x| \le W/2 \text{ and } |y| \le W/2 \end{cases}$$

$$\boldsymbol{j}_p^6(\boldsymbol{\rho}) := \begin{cases} \hat{x}A_p(x,-y) & x > W/2 \\ \hat{y}A_p(-y,x) & y < -W/2 \\ \hat{x}c(-x)s(y) + \hat{y}s(-x)c(y) & |x| \le W/2 \text{ and } |y| \le W/2 \end{cases}$$

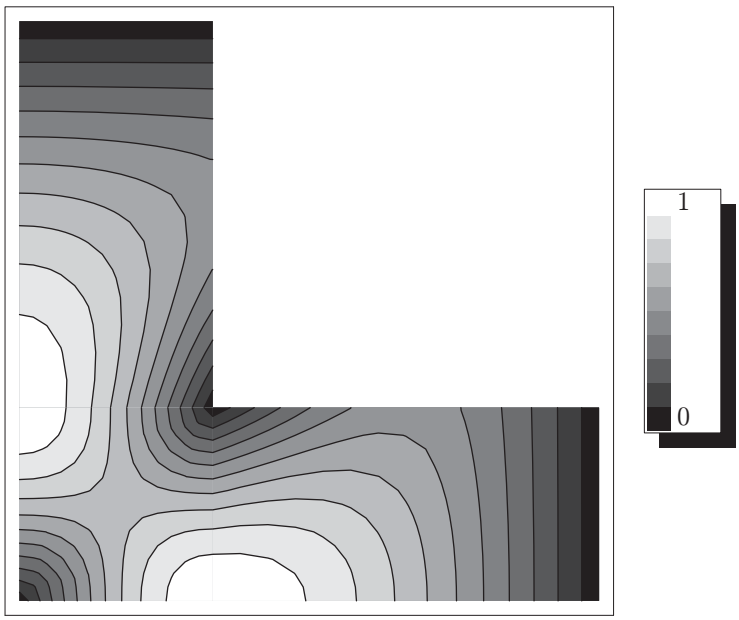

Figure 5: The amplitude of the V-dipole basis function $\boldsymbol{j}_1^3(\boldsymbol{\rho})$.

where the arm function $A_p(x, y)$ is defined through

$$A_p(x, y) := u_p(x)[c(y) - v(x)(c(y) - 1)]$$

and where

$$\begin{aligned} u_p(x) &:= \sin\big(\pi(2p-1)(x + L/2 - W)/(L - W)\big) \\ v(x) &:= \sin\big(\pi(x - W/2)/(L - W)\big) \\ s(\xi) &:= \sin\big(\pi(\xi + W/2)/2W\big) \\ c(\xi) &:= \cos\big(\pi(\xi + W/2)/2W\big) \end{aligned}$$

These V-dipole basis functions approximate the surface current density in 90° V-dipoles that gives the second resonance at f_2. Roughly speaking, if we bend either $\boldsymbol{j}_p^1(\boldsymbol{\rho})$ or $\boldsymbol{j}_p^2(\boldsymbol{\rho})$ 90° at the center of the cross, we obtain the V-dipole basis functions. Figure 5 shows the amplitude of the V-dipole basis function $\boldsymbol{j}_1^3(\boldsymbol{\rho})$, *i.e.*, $|\boldsymbol{j}_1^3(\boldsymbol{\rho})|$ is plotted as a function of the spatial coordinates x and y. Note that the V-dipole basis functions are continuous, even at the center of the cross, see Figure 6. Since the V-dipole basis functions are comprised of ordinary sines and cosines, they are easy to Fourier transform. We use the following enumeration of the basis functions,

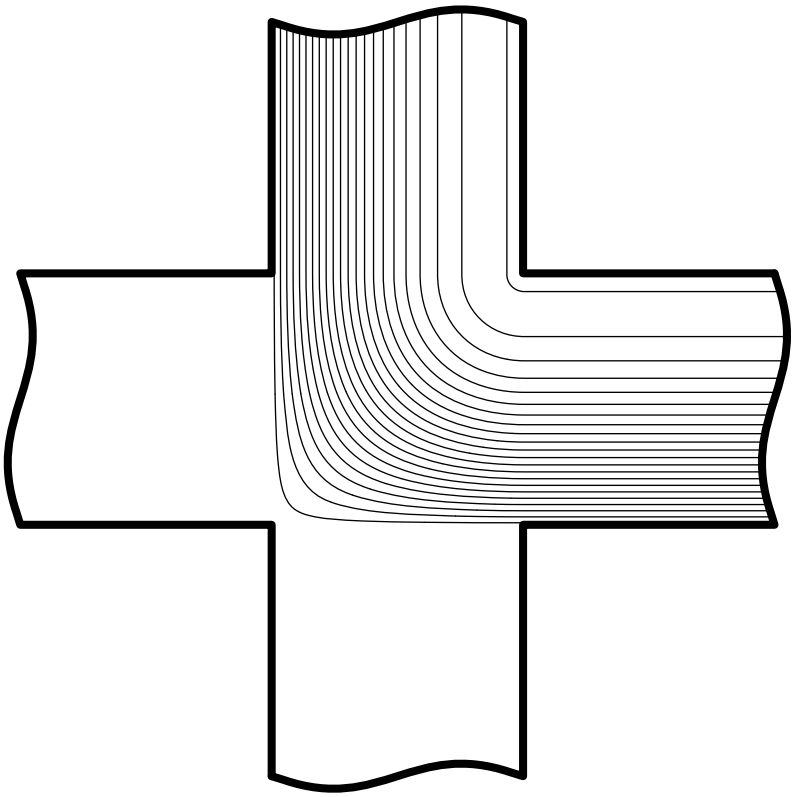

Figure 6: The current lines at the center of the cross.

i.e., the index is mod 6,

$$\boldsymbol{j}_p(\boldsymbol{\rho}) := \begin{cases} \boldsymbol{j}^1_{(p+5)/6}(\boldsymbol{\rho}) & p = 1, 7, 13, \ldots \\ \boldsymbol{j}^2_{(p+4)/6}(\boldsymbol{\rho}) & p = 2, 8, \ldots \\ \boldsymbol{j}^3_{(p+3)/6}(\boldsymbol{\rho}) & p = 3, 9, \ldots \\ \boldsymbol{j}^4_{(p+2)/6}(\boldsymbol{\rho}) & p = 4, 10, \ldots \\ \boldsymbol{j}^5_{(p+1)/6}(\boldsymbol{\rho}) & p = 5, 11, \ldots \\ \boldsymbol{j}^6_{p/6}(\boldsymbol{\rho}) & p = 6, 12, \ldots \end{cases}$$

These basis functions can straightforwardly be generalized to cover crossed dipoles with unequal lengths and widths of the arms.

3.2 The spatial Fourier transform

The spatial Fourier transform of the traditional dipole basis functions in (3.1) is easily obtained. If we introduce the function

$$\tilde{j_p^1}(\alpha,\beta) := LW(-1)^{p+1}(\Gamma_1(\alpha)+\Gamma_1(-\alpha))\Gamma_2(\beta)/2$$

where $\Gamma_1(\eta) := \mathrm{sinc}(\pi(2p-1)/2+\eta L/2)$ and $\Gamma_2(\eta) := \mathrm{sinc}(\eta W/2)$, we have

$$\tilde{\boldsymbol{j}_p^1}(\boldsymbol{\rho}) = \hat{x}\tilde{j_p^1}(\alpha,\beta) \qquad \tilde{\boldsymbol{j}_p^2}(\boldsymbol{\rho}) = \hat{y}\tilde{j_p^1}(\beta,\alpha)$$

The following transform is useful when we determine the transform of the V-dipole basis functions,

$$\tilde{c}(\eta) := \int_{-W/2}^{W/2} c(\xi)e^{-i\eta\xi}\,d\xi = \frac{W}{2}\left(\frac{1-i}{\sqrt{2}}\Gamma_3(\eta)+\frac{1+i}{\sqrt{2}}\Gamma_3(-\eta)\right)$$

where $\Gamma_3(\eta) := \mathrm{sinc}(\pi/4+\eta W/2)$. Similarly, we have

$$\tilde{s}(\eta) := \int_{-W/2}^{W/2} s(\xi)e^{-i\eta\xi}\,d\xi = \tilde{c}^*(\eta)$$

Yet another useful transform is

$$\tilde{u}_p(\eta) := \int_{W/2}^{L/2} u_p(\xi)e^{-i\eta\xi}\,d\xi = \frac{i(-1)^p e^{-i\eta W/2}-e^{-i\eta L/2}\Gamma_4}{\eta(1-\Gamma_4^2)}$$

where $\Gamma_4 := (2p-1)\pi/\eta(L-W)$. Finally, we also make use of the transform

$$\tilde{w}_p(\eta) := \int_{W/2}^{L/2} u_p(\xi)v(\xi)e^{-i\eta\xi}\,d\xi = \Psi(L/2)-\Psi(W/2)$$

where

$$\begin{aligned}
\Psi(\xi) &:= \frac{\Psi^+(\xi)+\Psi^-(\xi)}{4}\\
\Psi^\pm(\xi) &:= \left(\Lambda_{p-1}^\pm(\xi)e^{\pm i\pi W/(L-W)}-\Lambda_p^\pm(\xi)\right)e^{\pm\Gamma_5}\\
\Lambda_p^\pm(\xi) &:= \frac{e^{i\xi(-\eta\pm 2\pi p/(L-W))}}{i(-\eta\pm 2\pi p/(L-W))}\\
\Gamma_5 &:= i\pi\left(p\left(1-\frac{W}{L-W}\right)-\frac{1}{2}\right)
\end{aligned}$$

Now, introducing the functions

$$\begin{aligned}
\tilde{j_p^3}(\alpha,\beta) &:= \tilde{A}_p(\alpha,\beta)+\tilde{s}(\alpha)\tilde{c}(\beta)\\
\tilde{j_p^4}(\alpha,\beta) &:= -\tilde{A}_p(-\alpha,-\beta)-\tilde{c}(\alpha)\tilde{s}(\beta)\\
\tilde{j_p^5}(\alpha,\beta) &:= -\tilde{A}_p(-\alpha,\beta)-\tilde{s}(-\alpha)\tilde{c}(\beta)\\
\tilde{j_p^6}(\alpha,\beta) &:= \tilde{A}_p(\alpha,-\beta)+\tilde{c}(-\alpha)\tilde{s}(\beta)
\end{aligned}$$

where $\tilde{A}_p(\alpha,\beta) := (\tilde{u}_p(\alpha) - \tilde{w}_p(\alpha))\tilde{c}(\beta) + \tilde{w}_p(\alpha)\Gamma_2(\beta)$, the Fourier transform of the V-dipole basis functions can be written

$$\tilde{\boldsymbol{j}}_p^n(\alpha,\beta) = \hat{x}\tilde{j}_p^n(\alpha,\beta) - \hat{y}\tilde{j}_p^n(\beta,\alpha) \quad n = 3,4$$
$$\tilde{\boldsymbol{j}}_p^n(\alpha,\beta) = \hat{x}\tilde{j}_p^n(\alpha,\beta) + \hat{y}\tilde{j}_p^n(-\beta,-\alpha) \quad n = 5,6$$

Note the symmetry in α and β.

3.3 The geometry of Tsao and Mittra

In this section we consider the geometry of Tsao and Mittra [17], *i.e.*, $a = 24.40$ mm, $b = 17.25$ mm, $L = 15.10$ mm, $W = 0.44$ mm, and $\phi_0 = 45°$. Actually, this geometry also occurs in the paper of Pelton and Munk [14], and they have included measured data, which we use for comparison in our calculations.

In this paper we use the Z matrix interpolation method, recently presented by Barlevy [2]. We calculate the matrix $\mathbf{A}$ in the linear system (2.13b) at the frequencies 8, 9, 10, 11 and 12 GHz and store them. Then, we compute the intermediate frequency values of the matrix elements a_{pq} by cubic spline interpolation, and solve for the current coefficients C_p. Hence, to get the reflection and transmission coefficients of the FSS, for all frequencies at the X-band (8–12 GHz), we only need to calculate the matrix $\mathbf{A}$ at 5 frequencies.

Figure 7 depicts the (power) reflection coefficient for TM incidence, as a function of frequency and the number of odd dipole basis functions [17] included. The angles of incidence are chosen as $\theta = 60°$ and $\phi = 0°$. The number of even dipole basis functions included is 4, *i.e.*, 2 on each arm. Moreover, the double infinite Floquet sum is truncated as $\sum_{m=-N}^{N}\sum_{n=-N}^{N}$, where $N = 400$. Hence, the number of Floquet modes included is 801^2. This truncation is determined by adding Floquet modes until the result does not change. From Figure 7 it is concluded that, for this geometry, it is adequate to include about 100 odd dipole basis functions; fewer basis functions do not localize the second resonance at f_2 correctly. However, the ill-posed nature of the underlying integral equation shows up if too many basis functions are used, *cf.*, Figure 8, which depicts the condition number, defined as the ratio of the largest singular value to the smallest one, of the matrix $\mathbf{A}$ of the linear system (2.13b). Due to computer time limitations, we have not been able to examine whether the odd dipole solution, Figure 7, do converge or stabilize when more than 200 basis functions are included.

The condition number depicted in Figure 8 needs a few more comments. The machine epsilon M_ϵ [5] is a common measure of computing precision. By definition the machine epsilon is the smallest floating point number with the property that $1 + M_\epsilon > 1$. Loosely speaking, a linear system is well conditioned with respect to the computing precision if the condition number is small relative to $1/M_\epsilon$ [5]. All computations in this paper was performed in double precision, on a PC where the machine epsilon is approximately given by $1/M_\epsilon = 10^{16}$. Hence, from Figure 8 it is concluded that the linear system (2.13b) is well conditioned with respect to the computing precision for the computations of the reflection coefficients depicted in Figure 7.

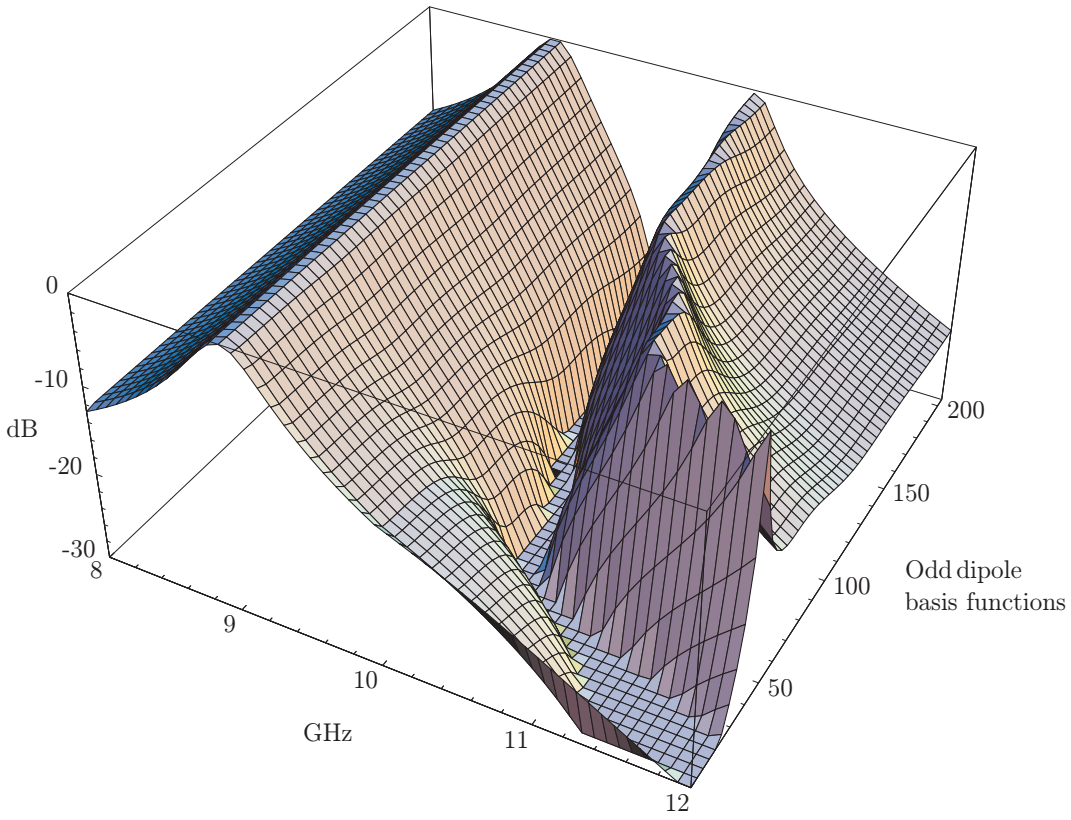

Figure 7: The power reflection coefficient for TM incidence as a function of frequency (8–12 GHz) and the number of odd dipole basis functions included (0–200).

Figure 9 shows the (power) reflection coefficient for TM incidence as a function of frequency. Three curves are drawn in this figure. Firstly, the solid curve with black dots, is measured and originates from Pelton and Munk [14]. The points are the measure points. Secondly, the dashed curve is computed with 4 even dipole basis functions and 100 odd dipole basis functions. Finally, the solid curve is computed with 2 even dipole basis functions and 2 V-dipole basis functions. The number of Floquet modes included for the computation of the dashed and solid curve is 201^2 and 31^2, respectively. Due to to the larger number of basis functions required, 100 versus 4, and the number of Floquet modes required, the V-dipole basis functions are definitely preferable compared to the odd dipole basis functions. In fact, it is found that the computation time per frequency when the V-dipole basis functions are used is reduced to about 0.06% of the computation time when the odd dipole

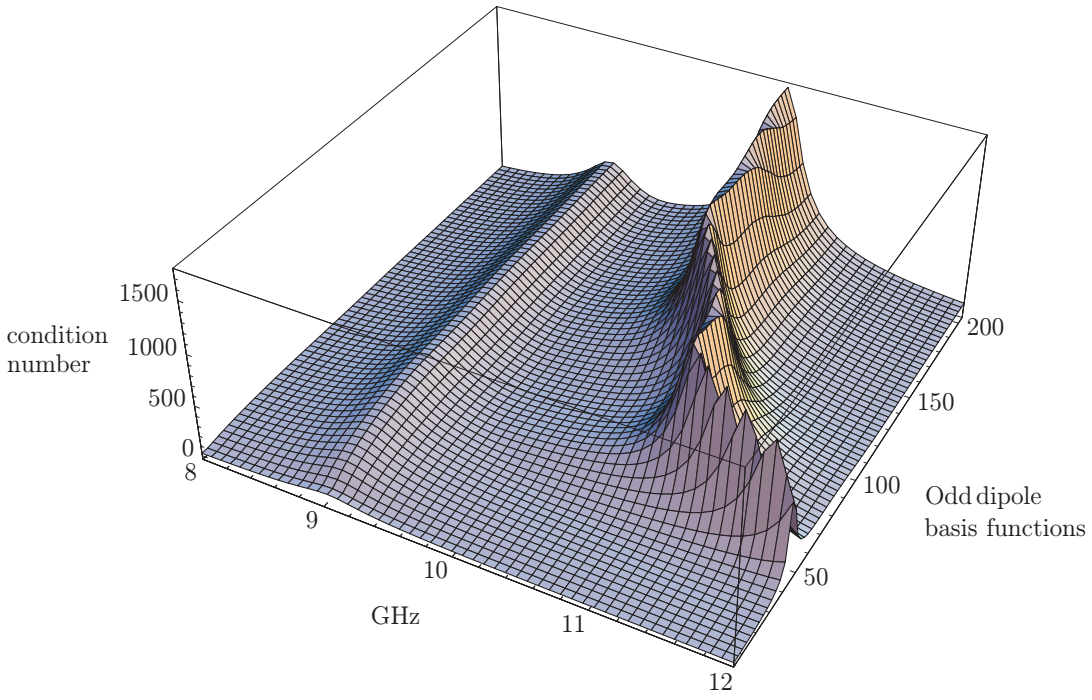

Figure 8: The condition number of the matrix **A** as a function of frequency (8–12 GHz) and the number of odd dipole basis functions included (0–200).

basis functions are used. This means that the computer code based on the V-dipole basis functions is about 1580 times faster than the corresponding code based on the odd dipole basis functions.

3.4 Crosses with unequal length of the arms

Recently the use of crossed dipoles with unequal length of the dipole arms in low observable, polarisation twisting, reflector antennas was proposed [4]. In this section, the effect of reducing the length of one of the dipole arms is demonstrated.

We denote the length of the arm parallel to the x and y-axis by L_x and L_y, respectively, see Figure 4. In the previous section $L_x = L_y$, but here we consider crossed dipoles with unequal length of the arms, *e.g.*, $L_x > L_y$. For comparing reasons, we consider the same geometry as above, but the length of the y-arm is reduced to $L_y = 13.1$ mm. However, the length of the x-arm is $L_x = 15.1$ mm, as above, see Figure 10. In Figure 11, a plot depicting the (power) reflection coefficient for TM incidence, as a function of frequency and the number of odd basis functions included, is given. The angles of incidence are chosen as $\theta = 60^\circ$ and $\phi = 0^\circ$. The number of even dipole basis functions included is 4, *i.e.*, 2 on each arm. Moreover, 401^2 Floquet modes are included. From Figure 7 and 11 we conclude that the second resonance at f_2 still occurs when the dipole arms have unequal length, and that the second resonance occurs at a higher frequency when L_y is reduced. It is also concluded that the first resonance at f_1 remains unaltered when the length L_y

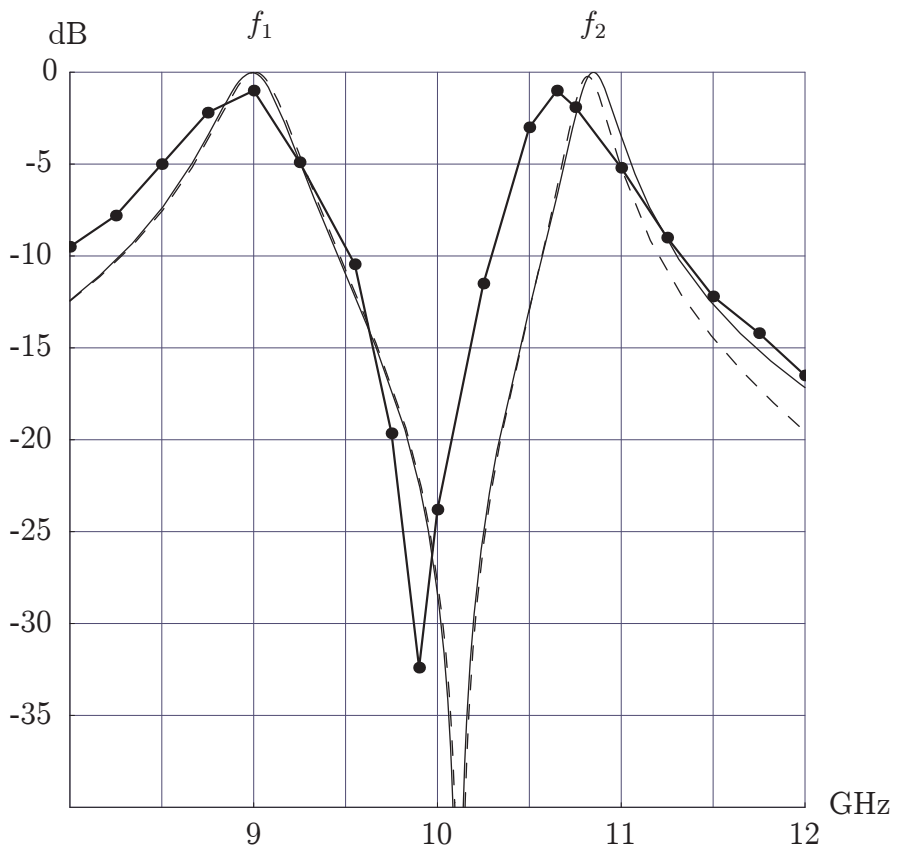

Figure 9: The power reflection coefficent for TM incidence as a function of frequency. The solid curve with black dots is measured [14]. The dashed curve is computed with 4 even dipole basis functions and 100 odd dipole basis functions. The solid curve is computed with 2 even dipole basis functions and 2 V-dipole basis functions.

is reduced.

Finally, Figure 12 shows the (power) reflection coefficient for TM incidence for the same geometry as above, *i.e.*, the geometry given in Figure 10. The angles of incidence are chosen as $\theta = 60^\circ$ and $\phi = 0^\circ$. The dashed curve is computed with 4 even dipole basis functions and 80 odd dipole basis functions. Moreover, the solid curve is computed with 2 even dipole basis functions and 2 V-dipole basis functions. The number of Floquet modes included for the computation of the dashed and solid curve is 161^2 and 31^2, respectively. It is found that the computation time per frequency when the V-dipole basis functions are used is reduced to about 0.15% of the computation time when the odd dipole basis functions are used. This means that the computer code based on the V-dipole basis functions is about 660 times faster than the corresponding code based on the odd dipole basis functions.

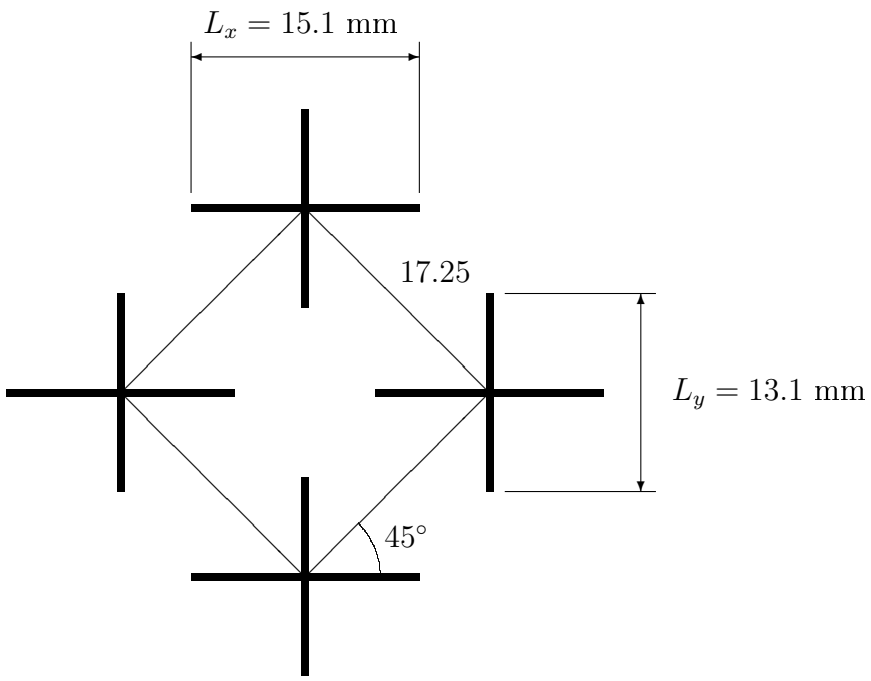

Figure 10: Crossed dipoles with unequal length of the dipole arms.

4 Conclusions

In this paper the reflection and transmission properties of an infinite array of crossed dipoles have been analyzed by the use of the spectral Galerkin method. A thorough treatment of the continuity condition is presented in the paper and, moreover, the analysis shows that the junction basis function given by Tsao and Mittra [17] are impertinent.

The continuity condition applies to all entire domain basis functions used in the spectral Galerkin method. Since the junction basis function of Tsao and Mittra cannot be used, and the MoM solution with odd dipole basis functions converges very slowly, the need for an improved set of basis functions for crossed dipoles is obvious. To this end, we presented a set of V-dipole basis functions, which together with the ordinary even dipole basis functions form an excellent system of basis functions for crossed dipoles. It was found that only 4 of the presented basis functions gave highly accurate results, even above the first resonance at f_1. We have considered both crossed dipoles with equal and unequal length of the dipole arms. Finally, the effect of reducing the length of one arm only was demonstrated.

However, the presented basis functions do not satisfy the edge condition, which requires that the current component parallel to an edge must be singular. It is not known how this edge condition changes these results concerning convergence of the MoM solution, number of Floquet modes needed, etc. However, it is expected that basis functions with correct edge behaviour improves the convergence [1].

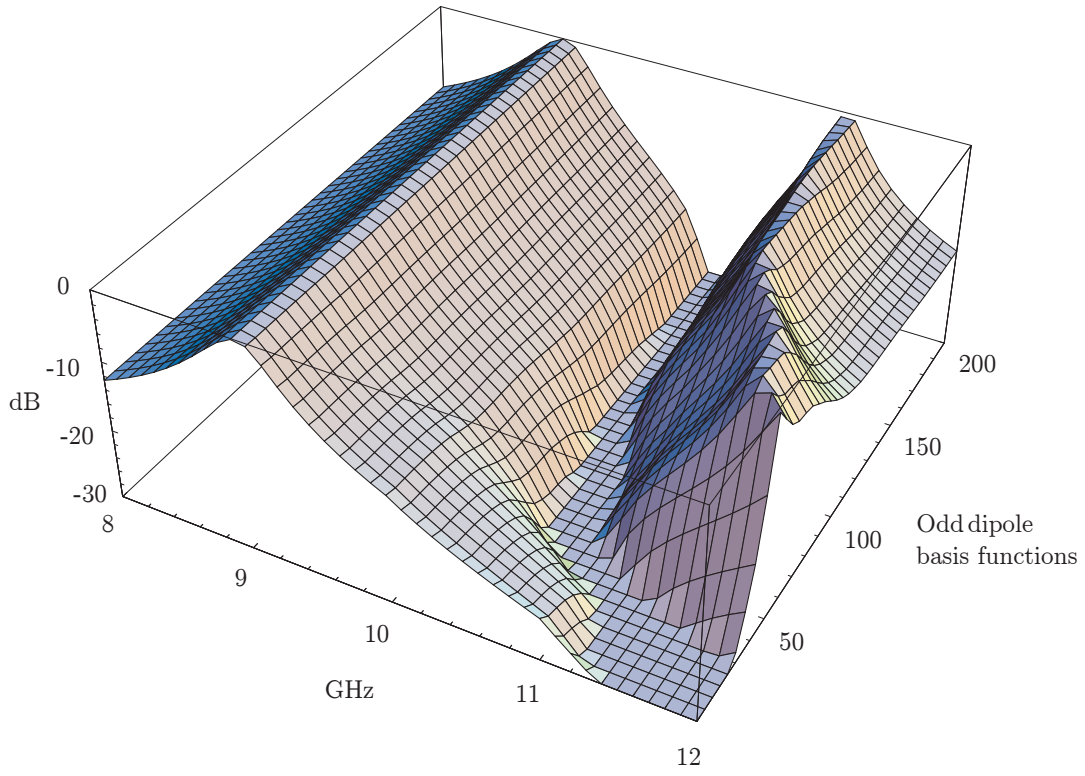

Figure 11: The power reflection coefficient for TM incidence as a function of frequency (8–12 GHz) and the number of odd dipole basis functions included (0–200). The length of the y-arm is reduced to $L_y = 13.1$ mm.

The extension of the given V-dipole basis functions to adopt the Jerusalem cross [13] is straightforward. However, the generalization of the given V-dipole basis functions to non right angle V-dipoles, with applications on tripoles, is not obvious.

5 Acknowledgments

I would like to thank my supervisor prof. Gerhard Kristensson for his excellent guidance throughout this work. I am deeply grateful to doc. Börje Nilsson for the many valuable discussions. I am also deeply grateful to prof. Per-Simon Kildal for his support concerning the G1DMULT routine, which excellently take care of any dielectric support of the FSS.

Finally, I would like to thank Applied Composites AB ACAB for financial support.

References

[1] T. Andersson. Moment-method calculations on apertures using basis singular functions. *IEEE Trans. Antennas Propagat.*, **41**(12), 1709–1716, 1993.

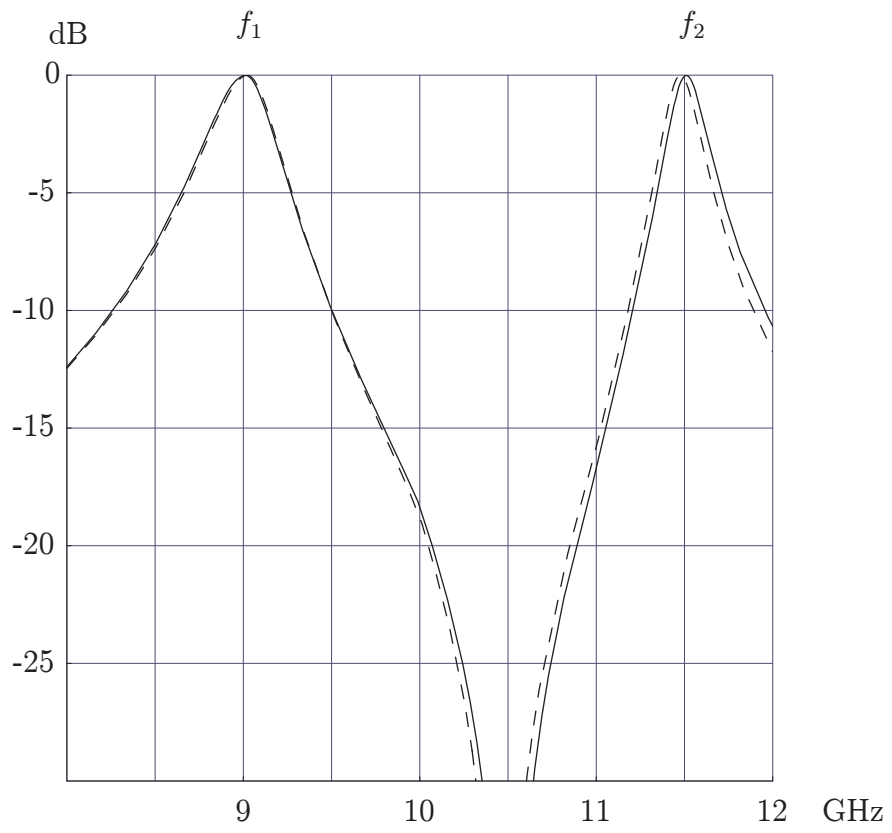

Figure 12: The power reflection coefficent for TM incidence as a function of frequency. The dashed curve is computed with 4 even dipole basis functions and 100 odd dipole basis functions. The solid curve is computed with 2 even dipole basis functions and 2 V-dipole basis functions. The length of the y-arm is reduced to $L_y = 13.1$ mm.

[2] A. S. Barlevy. *Properties of electromagnetic scattering from periodic metallic structures: Applications to frequency selective and bandgap structures.* PhD thesis, University of California, 1998.

[3] D. Colton and R. Kress. *Integral Equation Methods in Scattering Theory.* John Wiley & Sons, New York, 1983.

[4] O. Forslund and P. Sjöstrand. A flat reflector antenna with low radar cross section. In *International Radar Symposium*, volume I, pages 303–311, Munich, Germany, 15–17 September 1998.

[5] W. W. Hager. *Applied numerical linear algebra.* Prentice-Hall, Inc., Englewood Cliffs, New Jersey, 1988.

[6] S. M. A. Hamdy and E. A. Parker. Influence of lattice geometry on transmission of electromagnetic waves through arrays of crossed dipoles. *IEE Proc.-H Microwaves, Antennas and Propagation*, **129**(1), 7–10, February 1982.

[7] A. Ishimaru. *Electromagnetic Wave Propagation, Radiation, and Scattering.* Prentice-Hall, Inc., Englewood Cliffs, New Jersey, 1991.

[8] F. S. Johansson. Convergence phenomenon in the solution of dichroic scattering problems by Galerkin's method. *IEE Proc.-H Microwaves, Antennas and Propagation*, **134**, 87–92, February 1987.

[9] P.-S. Kildal, Z. Šipuš, and M. Johansson. A numerical algorithm G1DMULT for computing Green's functions of multilayer objects. Technical report, Chalmers University of Technology, Dep. of Microwave Technology, 1997.

[10] R. W. P. King and B. H. Sandler. Analysis of the currents induced in a general wire cross by a plane wave incident at an angle with arbitrary polarization. *IEEE Trans. Antennas Propagat.*, **29**(3), 512–520, May 1981.

[11] R. A. Kipp and C. H. Chan. A numerically efficient technique for the method of moments solution for planar periodic structures in layered media. *IEEE Trans. Microwave Theory Tech.*, **42**(4), 635–643, 1994.

[12] J. M. Ortega. *Matrix Theory (A Second Course).* Plenum Press, New York, 1987.

[13] E. A. Parker, S. M. A. Hamdy, and R. J. Langley. Modes of resonance of the Jerusalem cross in frequency-selective surfaces. *IEE Proc.-H Microwaves, Antennas and Propagation*, **130**(3), 203–208, April 1983.

[14] E. L. Pelton and B. A. Munk. Scattering from periodic arrays of crossed dipoles. *IEEE Trans. Antennas Propagat.*, **27**(3), 323–330, 1979.

[15] N. V. Shuley. A note on relative convergence for moment-method solutions of integral equations of the first kind as applied to dichroic problems. *Electronics Letters*, **21**(3), 95–97, 1985.

[16] I. Stakgold. *Green's Functions and Boundary Value Problems.* John Wiley & Sons, New York, 1979.

[17] C.-H. Tsao and R. Mittra. Spectral-domain analysis of frequency selective surfaces comprised of periodic arrays of cross dipoles and Jerusalem crosses. *IEEE Trans. Antennas Propagat.*, **32**(5), 478–486, 1984.

[18] J. C. Vardaxoglou. *Frequency Selective Surfaces (Analysis and Design).* Research Studies Press, 1997.

[19] T. K. Wu, editor. *Frequency Selective Surface and Grid Array.* John Wiley & Sons, New York, 1995.